American Mineralogist, Volume 97, pages 1915–1921, 2012

Synthesis and crystal chemistry of Fe^{3+}-bearing $(Mg,Fe^{3+})(Si,Fe^{3+})O_3$ perovskite

Daniel R. Hummer* and Yingwei Fei

Geophysical Laboratory, Carnegie Institution of Washington, Washington, D.C. 20015, U.S.A.

Abstract

We have synthesized magnesium-iron silicate perovskites with the general formula $Mg_{1-x}Fe^{3+}_{x+y}Si_{1-y}O_3$, in which the iron cation is exclusively trivalent. To investigate the crystal chemistry of Fe^{3+}-bearing perovskite, six samples (both with and without Al) were analyzed using scanning electron microscopy, electron microprobe, X-ray diffraction, and Mössbauer spectroscopy. Results indicate that Fe^{3+} substitutes significantly into both the octahedral and dodecahedral sites in the orthorhombic perovskite structure, but prefers the octahedral site at Fe^{3+} concentrations between 0.04 and 0.05 Fe per formula unit, and the dodecahedral site at higher Fe^{3+} concentrations. We propose a model in which Fe^{3+} in the A/B site (in excess of that produced by charge coupled substitution) is accommodated by Mg/O vacancies. Hyperfine parameters refined from the Mössbauer spectra also indicate that a portion of dodecahedral sites undergo significant structural distortion. The presence of Fe^{3+} in the perovskite structure increases the unit-cell volume substantially compared to either the Mg end-member, or Fe^{2+}-bearing perovskite, and the addition of Al did not significantly alter the volume. Implications for increased compressibility and a partially suppressed spin transition of Fe^{3+} in lower mantle perovskite are also discussed.

Keywords: Perovskite, ferric iron, lower mantle, oxidation state, diffraction, Mössbauer, crystal chemistry

Introduction

Magnesium silicate perovskite, $MgSiO_3$ (hereafter referred to as Mg-Pv), is thought to comprise ~40% of the Earth by volume and is widely accepted to be the dominant mineral phase in the Earth's mantle (Fei and Bertka 1999). Iron is among the most important elements that substitutes into the perovskite structure, and is especially important in the lower mantle because it affects density and elastic properties. The substitution of Fe^{2+} into Mg-Pv to form $(Mg,Fe)SiO_3$, and its impacts on material properties, have been extensively studied (e.g., Knittle and Jeanloz 1987; Kudoh et al. 1990; Parise et al. 1990; Fei et al. 1994; Martinez et al. 1997; Lundin et al. 2008; Hsu et al. 2010).

However, recent experimental results suggest a disproportionation reaction of Fe^{2+} into Fe^{3+} and metallic Fe that may cause the lower mantle, despite having a much lower oxygen fugacity than the crust or upper mantle, to contain $Fe^{3+}/\Sigma Fe$ ratios as high as 0.60. Evidence for this reaction has been observed at 25–26 GPa in the multi-anvil press (Lauterbach et al. 2000; Frost et al. 2004), and at pressures ranging from 55 to 100 GPa in the diamond-anvil cell (Auzende et al. 2008). Theoretical calculations show that the disproportionation should be strongly exothermic throughout the lower mantle (Zhang and Oganov 2006). Experiments on lower mantle mineral assemblages have yielded $Fe^{3+}/\Sigma Fe$ ratios up to 0.8 in Mg-Pv, depending on the total concentrations of Fe and Al (McCammon et al. 2004). Furthermore, Fe^{3+} is thought to partition strongly into the perovskite phase at lower mantle pressures (McCammon 1997). The chemical and mechanical properties of Fe^{3+}-bearing perovskite are therefore critical to our understanding of the composition and structure of the mantle.

Several studies have examined the role of Fe^{3+} in the Mg-Pv structure using samples with mixed valence Fe (McCammon 1997; Lauterbach et al. 2000; Frost and Langenhorst 2002; Frost et al. 2004; McCammon et al. 2004; Jackson et al. 2005; Grocholski et al. 2009). The major conclusions from these studies were that (1) significant Fe^{3+} can incorporate into Mg-Pv, (2) the presence of Al increases the solubility of Fe^{3+} in Mg-Pv, and (3) Fe^{3+} can be accommodated in both the 8–12 coordinated (A) site, and the octahedrally coordinated (B) site in the perovskite structure, likely through a charge-coupled substitution (CCS) mechanism:

$$Mg^{2+}_A + Si^{4+}_B \rightarrow Fe^{3+}_A + Fe^{3+}_B. \quad (1)$$

Vanpeteghem et al. (2006a) concluded based on ex situ single-crystal diffraction measurements that Fe^{3+} occupies exclusively the A site when coupled with Al substitution into the B site. Alternatively, Catalli et al. (2011) propose that at high pressures, both Fe^{3+} and Al mix evenly between the A and B sites. However, these studies both used samples with significant concentrations of Fe^{2+} and/or Al, and the behavior of Fe^{3+} in Mg-Pv samples with $Fe^{3+}/\Sigma Fe$ close to 1 has scarcely been studied.

The first evidence for an end-member $(Mg,Fe^{3+})(Si,Fe^{3+})O_3$ perovskite phase with $Fe^{3+}/\Sigma Fe \sim 1$ was observed by Andrault and Bolfan-Casanova (2001) using in situ synchrotron X-ray diffraction. However, in those experiments the true composition and $Fe^{3+}/\Sigma Fe$ ratio of the perovskite phase were inferred from those of the starting material rather than being experimentally

* Present address: Department of Earth and Space Sciences, University of California Los Angeles, Los Angeles, California 90095, U.S.A. E-mail: dhummer@ess.ucla.edu

0003-004X/12/1112–1915$05.00/DOI: http://dx.doi.org/10.2138/am.2012.4144

verified. Catalli et al. (2010) synthesized the first Fe^{3+}-bearing Mg-Pv with $Fe^{3+}/\Sigma Fe = 1$, as measured by synchrotron Mössbauer spectroscopy (SMS). Those authors concluded based on SMS and X-ray emission spectroscopy (XES) measurements that Fe^{3+} occupancy was roughly equal between the A and B sites. These studies provide useful clues as to the role of Fe^{3+} in the Mg-Pv structure, but further study of ferric Mg-Pv samples with varying Fe concentrations is necessary to fully understand the crystallographic behavior of Fe^{3+} and assess its influence on critical properties of mantle perovskite. Furthermore, the only ferric Mg-Pv sample to date (Catalli et al. 2010) was synthesized in the laser-heated diamond-anvil cell with limited recoverability. Here we report a novel and reliable method of synthesis in the multi-anvil apparatus for >1 mm, Fe^{3+}-bearing Mg-Pv samples in which the Fe is exclusively trivalent, and draw conclusions regarding the crystallographic role of Fe^{3+} as a function of ΣFe.

Methods

Starting material was prepared from fired, reagent grade MgO, Fe_2O_3, SiO_2 and Al_2O_3 such that the Fe:(Mg+Fe) mole ratio was 0.05 or 0.10, and the (Mg+Fe) to Si mole ratio was 1:1. Mixed powders were ground in a mortar and pestle with ethanol for 60 min and then dried under a heat lamp for 30 min. Synthesis experiments were performed in a multi-anvil apparatus at the Geophysical Laboratory using a 1 mm OD Pt capsule in a large 8/3 cell assembly with Re heater (Bertka and Fei 1997). The powdered oxide mixtures with all ferric iron were sealed in Pt capsules. A layer of hematite (Fe_2O_3) was packed between the Pt capsule and the Re heater to maintain a high f_{O_2} within each sample capsule, and ensure that all sample Fe remained oxidized. Samples were heated for ~12 h at 1700–1800 °C at a pressure of 25 GPa, and then quenched to preserve the perovskite phase. Temperature was measured with a C-type thermocouple (W-5%Re/W-26%Re) adjacent to the sample capsule. In experiments for which a direct temperature reading from the thermocouple could not be obtained, temperature was estimated using the power-temperature relationship established for the sample assembly.

After quenching and depressurization, recovered samples were characterized at ambient conditions using powder X-ray diffraction, scanning electron microscopy, electron microprobe, and Mössbauer spectroscopy. Powder diffraction measurements were carried out on a Rigaku D/max Rapid microdiffractometer operated at 50 kV and 40 mA and equipped with an area detector using Mo*K*α radiation, and also at beamline 13-ID-D (GSECARS) at the Advanced Photon Source, Argonne National Laboratory. For two samples, single-crystal diffraction measurements were collected using an Oxford SuperNova instrument equipped with an Atlas CCD detector and Mo*K*α radiation at the Virginia Tech Crystallography Laboratory. Powder diffraction patterns were analyzed with the Rietveld technique using the GSAS software package (Larson and Von Dreele 2000).

Images and EDS spectra were collected on a field emission JEOL JSM-6500F scanning electron microscope operated at 15 kV. Chemical compositions were analyzed with a JEOL JXA-8900 microprobe operated at 15 kV and 30 nA using enstatite and almandine standards. Mössbauer measurements were made using a custom-built spectrometer with a ^{57}Co γ source, and the velocity scale was calibrated using ^{57}Fe foil. Crushed powders were spread into a thin, <1 mm layer in the center of a copper sample holder and placed ~3 inches from the γ source. The resulting Mössbauer spectra were background corrected and fit to a three-doublet model using the open source refinement program Fit. A Lorentzian line shape was used for all doublets. The refinement was executed in random-walk mode, and each doublet was constrained to be symmetric. Isomer shifts and quadrupole splittings were estimated and refined first to model the recognizable peaks, and then intensity and line width were refined.

Results and Discussion

SEM and microprobe

SEM data showed that the run products consisted predominantly of a Mg-Pv phase, with small amounts of un-reacted MgO and SiO_2 (Fig. 1). X-ray diffraction data confirmed that both samples were predominantly the orthorhombic modification of the perovskite structure, with minor stishovite (Fig. 2), and will

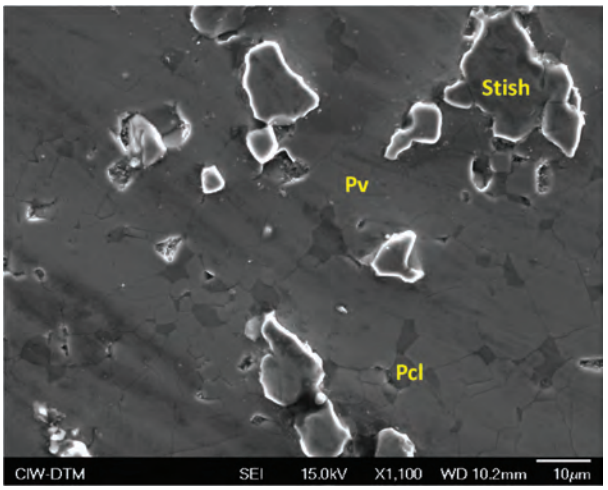

Figure 1. SEM micrograph of sample Pv05 taken at 15 kV with a magnification of 1100×. (Pv = perovskite; Pcl = periclase; Stish = stishovite). (Color online.)

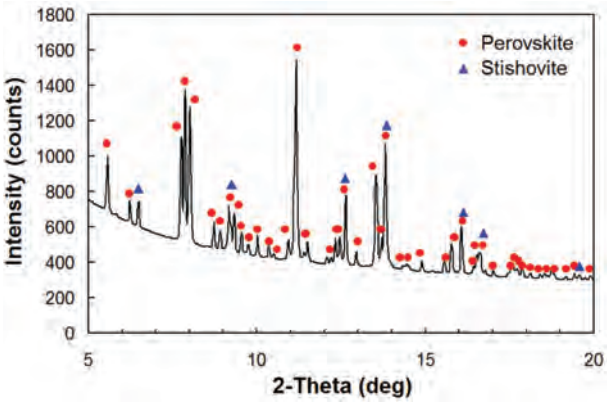

Figure 2. Powder X-ray diffraction scan of sample Pv05-57e, λ = 0.3344 Å (red circles = magnesium silicate perovskite peaks, blue triangles = stishovite peaks). This powder pattern was typical of all samples. (Color online.)

be discussed in more detail later in the text. All samples were translucent and pale yellow in color. Perovskite grains had an average diameter near 10 μm, while stishovite grains were up to 40 μm and periclase grains were much smaller (1–5 μm).

Electron microprobe compositions for the six samples are shown in Table 1. The fact that all of these compositions are charge balanced within the error of the measurements (assuming all Fe as Fe_2O_3) indicates that most Fe within the sample remained in the +3 valence state. In fact, in four out of six samples, the errors in the microprobe measurements constrained $Fe^{2+}/\Sigma Fe$ to be <0.13. The final $Fe^{3+}/\Sigma Fe$ ratio in the hematite buffer around the sample capsule was obtained by measuring the wt% Fe_2O_3 in the buffer, as well as in magnetite ($Fe^{3+}/\Sigma Fe = 0.666$) and hematite ($Fe^{3+}/\Sigma Fe = 1.000$) standards, and performing a linear interpolation. The observation that the hematite buffer retained a final $Fe^{3+}/\Sigma Fe$ ratio of at least 0.75 ± 0.1, as well as the absence of any Fe substitution in the un-reacted MgO observed by SEM, also support the inference that there was very little reduction of

TABLE 1. Microprobe compositions of six samples of $(Mg,Fe^{3+})(Si,Fe^{3+})O_3$ perovskite

	Pv05	Pv05-57e	Pv10	Pv05-05-57	Pv10-57	Pv05-57f
			Wt			
MgO	40.8(2)	40.8(2)	36.9(5)	38.0(1)	38.7(2)	39.61(8)
Fe_2O_3	3.6(1)	3.5(2)	5.9(4)	3.16(3)	3.9(2)	3.26(3)
SiO_2	58.6(3)	60.4(2)	59.0(6)	57.0(1)	57.7(3)	59.6(1)
Al_2O_3	–	–	–	2.76(5)	–	–
Total	103.1(2)	104.8(4)	101.9(2)	101.0(1)	100.4(2)	102.5(2)
			Cations per 3 O atoms			
Mg^{2+}	1.00(1)	0.984(2)	0.92(1)	0.949(2)	0.975(4)	0.974(2)
Fe^{3+}	0.045(2)	0.043(2)	0.074(5)	0.0399(4)	0.050(2)	0.0405(4)
Si^{4+}	0.965(3)	0.975(1)	0.984(8)	0.955(1)	0.975(3)	0.983(1)
Al^{3+}	–	–	–	0.0546(9)	–	–
Net formula charge	0.00(1)	0.001(9)	0.00(4)	0.002(6)	0.00(2)	0.002(6)

Notes: Values in parentheses represent the mean standard error in the final digit of the measurement—mean standard error was calculated as $\varepsilon = \sigma/n^{1/2}$, where σ is the standard deviation of the measurements, and n is the number of measurements. The errors in the raw measurements were propogated to the net formula charge using the standard error propogation formula,

$$\varepsilon_x = \sqrt{\varepsilon_a^2\left(\frac{\partial x}{\partial a}\right)^2 + \varepsilon_a^2\left(\frac{\partial x}{\partial a}\right)^2 + \ldots},$$

where x is the net formula charge and a, b, etc. are the raw measurements for each element.

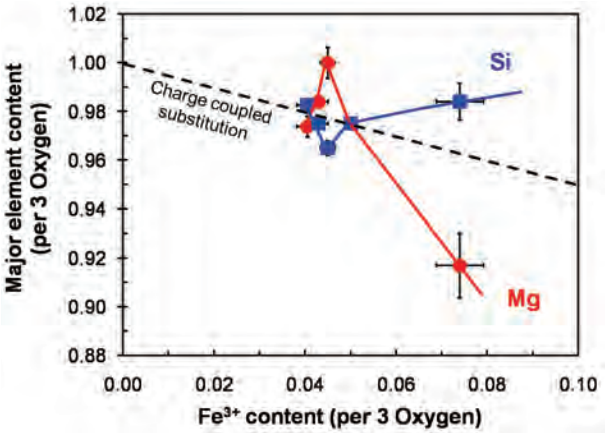

FIGURE 3. Average Mg (red circles) and Si (blue squares) microprobe concentrations in Fe^{3+}-bearing Mg-Pv as a function of average Fe^{3+} content. Error bars represent 1σ uncertainties of the mean, and were calculated as $\sigma/n^{1/2}$, where σ is the standard deviation of the measurements and n is the number of measurements. The dashed line represents theoretical concentrations of both Mg and Si assuming only a charge coupled substitution mechanism for Fe^{3+} (i.e., equal substitution of Fe^{3+} into the A and B sites). (Color online.)

Fe within the sample. The total concentration of Fe measured by microprobe analysis in each run product was lower than that of the starting material. We attribute this to the diffusion of Fe into the Pt capsule during synthesis, as found in similar experiments (Kudoh et al. 1990; Parise et al. 1990).

Examination of the measured Mg and Si concentrations in perovskites with different Fe^{3+} content provides constraints on the location of Fe^{3+} in the perovskite structure (Fig. 3). Perovskites containing between 0.04 and 0.05 Fe^{3+} per formula unit possessed high Mg concentrations and somewhat lower Si concentrations, indicating that in these samples, most Fe^{3+} substitutes for Si in the B site. However, samples with >0.05 Fe^{3+} per formula unit yielded larger Si concentrations and lower Mg concentrations, indicating that more Fe^{3+} substitutes for Mg in the A site. These results are consistent with previous studies indicating that Fe^{3+} can occupy both sites (McCammon 1997; Catalli et al. 2010), but also suggests a systematic trend in occupancy as a function of Fe content. The facts that (1) the observed occupancy trend is substantially larger than the error of the microprobe measurements, and (2) the same trend in Fe^{3+} occupancy is reflected in both the Mg concentrations and the independently measured Si concentrations, suggest that the trend is a real crystallographic effect rather than an artifact of random error.

For a sample to have Mg > Si requires some Fe^{3+} to substitute into the B site through a mechanism other than charge-coupled substitution (CCS). A single Fe^{3+} ion replacing a Si^{4+} in the B site can be charge balanced in one of only two ways: (1) an additional 1/2 Mg^{2+} in the A site, or (2) a 1/2 O^{2-} vacancy in the O site. Because one of these samples (Pv05) already has a Mg occupancy of 1.00 ± 0.01, it seems implausible that adding additional Mg is the correct substitution mechanism in this sample. Thus, we propose that when $Fe_B^{3+} > Fe_A^{3+}$, the excess Fe_B^{3+} (beyond that which is paired to Fe_A^{3+} via CCS) is accommodated by oxygen vacancies via the reaction

$$2Si_B^{4+} \rightarrow 2Fe_B^{3+} + V_O^{2+}. \quad (2)$$

Likewise, when Si > Mg, excess Fe^{3+} must substitute into the A site via a mechanism other than CCS. The excess positive charge can be charge balanced only by (1) 1/4 Si^{4+} vacancy, or (2) 1/2 Mg^{2+} vacancy. It is unlikely for a significant number of Si^{4+} vacancies to develop due to the unusually high concentration of negative charge each vacancy would produce. In addition, it would be vastly more favorable energetically to fill any Si^{4+} vacancies with Fe^{3+} to begin with (i.e., a substitution of $Fe_A^{3+}+Fe_B^{3+}$ should be greatly preferred over $2Fe_A^{3+}+1/2V_B$). Thus, we propose that at higher Fe^{3+} concentrations, excess Fe_A^{3+} is accommodated by Mg^{2+} vacancies via the reaction

$$3Mg_A^{2+} \rightarrow 2Fe_A^{3+} + V_A. \quad (3)$$

We note that sample Pv10-57, with Fe content precisely at the crossover point between these two mechanisms (Fe = 0.050) yielded a microprobe composition of $Mg_{0.975}Fe_{0.050}^{3+}Si_{0.975}SiO_3$, indicating a perfect CCS mechanism without excess Fe^{3+} in either crystallographic site.

A detailed analysis of sample Pv10, which had the highest Si occupancy (0.984) of our six samples, demonstrates that the above model is quantitatively consistent with the microprobe data. The maximum Fe^{3+} that can be accommodated in the B site in this sample is 0.016, which would pair with 0.016 Fe^{3+} in the A site via CCS, accounting for 0.032 of the Fe^{3+}. The remaining 0.074 – 0.032 = 0.042 of the Fe^{3+} must reside exclusively in the A site, which according to the stoichiometry of the above mechanism (Eq. 3), implies that $(3/2)\cdot 0.042 = 0.063$ of the Mg should be replaced (in addition to the 0.016 that was already replaced via CCS). The combined CCS/Mg vacancy model therefore yields a theoretical Mg occupancy of 1 – (0.016 + 0.063) = 0.921, which perfectly matches the 0.92(1) that was actually measured. This sample therefore shows evidence of precisely the right number of Mg vacancies to validate this model. Similar calculations show

that microprobe data for sample Pv05-57f are also quantitatively consistent with Equation 3, and that data for samples Pv05 and Pv05-57e are quantitatively consistent with Equation 2.

The trend in Fe^{3+} occupancy as a function of ΣFe can be understood in terms of the relevant crystal ionic radii of the constituent ions, which are 1.03 Å ($^{VIII}Mg^{2+}$), 0.92 Å ($^{VIII}Fe^{3+}$/high spin), 0.785 Å ($^{VI}Fe^{3+}$/high spin), and 0.540 Å ($^{VI}Si^{4+}$) (Shannon 1976). The crystal ionic radius of Fe^{3+} is therefore intermediate between those of Si^{4+} and Mg^{2+} assuming either coordination environment. However, Pauling's first rule of crystal structures (Pauling 1929) dictates that cations tend to occupy sites for which the cation/anion radius ratio will be above a certain minimum, to avoid loose cations and close contact between anions. The net strain is therefore minimized by initially allowing Fe^{3+} to substitute predominantly into the B site (with some offsetting substitution into the A site). As Fe^{3+} content increases, the increasingly positive strain in the octahedra is relieved by shifting occupancy to the A site, which has more space for the additional Fe^{3+} than does the already expanded B site.

However, for the deep mantle at pressures much larger than 25 GPa, it would be difficult to maintain a large number of Mg vacancies. Thus, although our data suggests that Fe^{3+} prefers increased A occupancy coupled with Mg vacancies at high Fe^{3+} content and ~25 GPa, the rise in pressure with increasing depth in the lower mantle may eventually force Fe^{3+} into a purely CCS mechanism. This idea is supported by the Fe^{3+} site occupancies measured by Catalli et al. (2010) using synchrotron Mössbauer spectroscopy, which yielded approximately equal occupancies for the A and B sites for pressures ≥47 GPa.

Mössbauer spectroscopy

Mössbauer spectra of ^{57}Fe-enriched samples of Fe^{3+}-bearing Mg-Pv could be fit to three doublets, all with small, positive isomer shifts (IS) relative to ^{57}Fe metal but with varying quadrupole splittings (QS) (Table 2). The experimental spectra and three-component fits are shown in Figure 4. The high IS, high QS doublet characteristic of Fe^{2+} in either 6- or 8-coordination, which typically has QS ~3.5 (Woodland and O'Neill 1993; Eeckhout et al. 2002; Geiger et al. 2003; Taran et al. 2007; Woodland et al. 2009) was completely absent from all spectra, further confirming that no Fe^{2+} was present in our samples.

The hyperfine parameters for the three components refined in this study are compared in Figure 5 with those of Fe^{2+} and Fe^{3+} in similar coordination environments as measured by other investigators. The M3 component, with IS = 0.298, 0.241, 0.328 mm/s and QS = 0.910, 1.011, 0.876 mm/s, plots close to Fe^{3+} in sixfold (octahedral) coordination. Furthermore, these values are in good agreement with those of McCammon et al. (2004), who measured an IS of ~0.3 mm/s and a QS of 0.73–0.94 mm/s for Fe^{3+} in Mg-Pv. With the exception of a somewhat smaller IS, these values also compare well with the IS (0.416, 0.414, 0.427 mm/s) and QS (0.993, 0.985, 0.927 mm/s) found by Fei

Table 2. Refined hyperfine Mössbauer parameters for two samples of Fe^{3+}-bearing perovskite and one sample of Fe^{3+} and Al-bearing perovskite (Pv05-05-57)

	Pv05-57f	Pv10-57	Pv05-05-57
M1 (Fe_A^{3+})			
IS	0.18	0.25	0.03
QS	0.32	0.55	0.33
Area(%)	18.8	17.0	20.4
M2 (Fe_A^{3+})			
IS	0.23	0.18	0.51
QS	1.60	1.70	1.43
Area(%)	38.2	31.8	22.4
M3 (Fe_B^{3+})			
IS	0.30	0.24	0.33
QS	0.91	1.01	0.88
Area (%)	43.0	51.2	57.2
M1:M2 area ratio	0.499	0.533	0.913
(M1+M2):M3 area ratio	57/43	51/49	43/57
A:B occupancy ratio*	58/42	50/50	–

Notes: These values are presented without errors because rather than being direct measurements, they are the optimized values yielding the best fit to the spectroscopic data using a least-squares refinement procedure that does not include error estimates. [IS = isomer shift relative to ^{57}Fe metal (mm/s); QS = quadrupole splitting (mm/s)].
* Inferred from microprobe data.

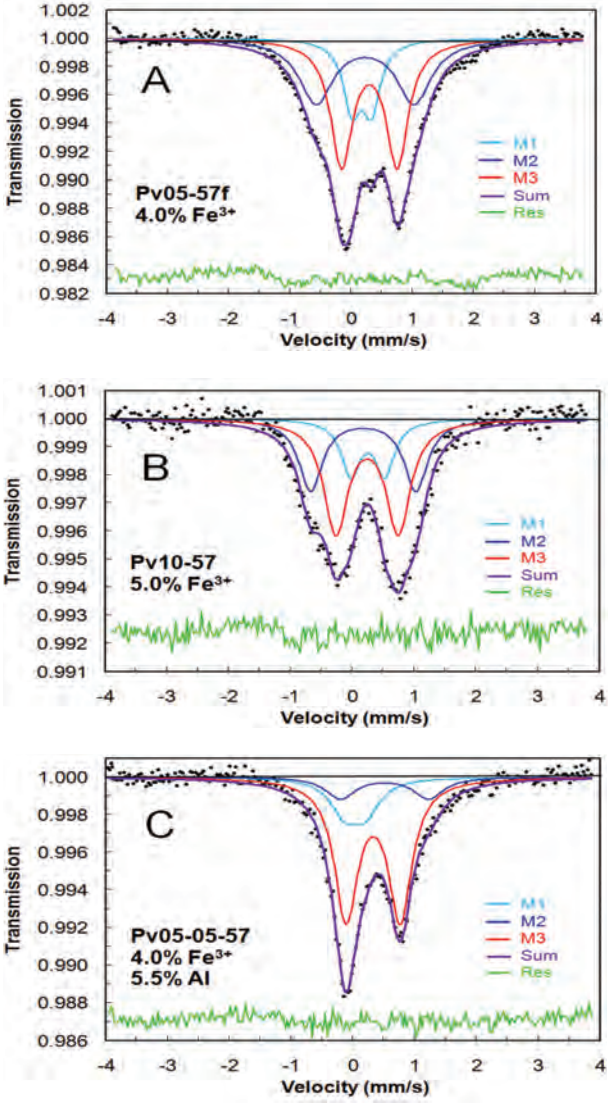

Figure 4. Mössbauer spectra for samples (**a**) Pv05-57f, (**b**) Pv10-57, and (**c**) Pv05-05-57. (Black dots = experimental data; light blue = M1 doublet; dark blue = M2 doublet; red = M3 doublet; purple = sum of all three doublets; green = residuals from model fit). (Color online.)

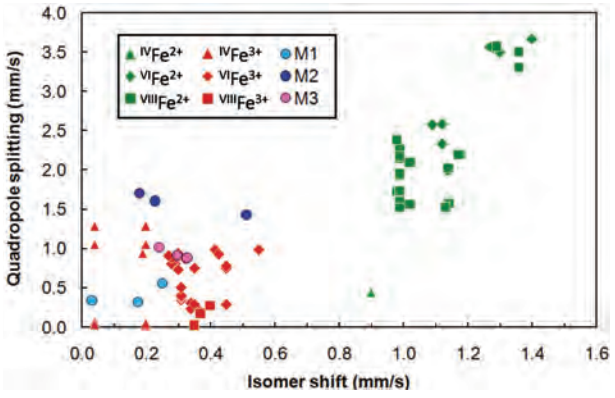

FIGURE 5. Mössbauer parameters from selected authors for 4-coordinated (triangles), 6-coordinated (diamonds), and 8-coordinated (squares) Fe^{2+} (green), and Fe^{3+} (red). Mössbauer parameters from this work are shown in circles for the M1 (light blue), M2 (dark blue), and M3 (pink) components. These values are presented without error bars because rather than being direct measurements, they are the optimized values yielding the best fit to the spectroscopic data as shown in the residuals in Figure 4. [Data sources: Amthauer et al. (1976), Woodland and O'Neill (1993), Fei et al. (1994), Eeckhout et al. (2002), Geiger et al. (2003), McCammon et al. (2004), Sharma et al. (2007), Taran et al. (2007), Grew et al. (2008), Woodland et al. (2009).] (Color online.)

et al. (1994) for the component attributed to octahedral Fe^{3+} in Mg-Pv. We therefore assign the M3 component in our spectra to Fe^{3+} in the perovskite B site.

The M1 component possesses the small QS characteristic of 8-coordinated Fe^{3+}, but has a significantly lower IS. However, a lower IS is consistent with the shorter bond distances of the more compact perovskite structure as compared to other 8-coordinated sites, such as those in the garnet structure (Sharma et al. 2007). We therefore assign the M1 component to Fe^{3+} in the perovskite A site. The M2 doublets have a similar IS to the M1 doublets, but have substantially larger QS. This phenomenon was also observed by Fei et al. (1994) and by McCammon et al. (2004) in the behavior of Fe^{2+} in the A site of Mg-Pv. Both studies fit the Mössbauer spectra of mixed valence (Mg,Fe)-Pv using two Fe^{2+} doublets having substantially different QS, and Fei et al. (1994) attributed these two doublets to dodecahedral sites with differing degrees of distortion.

Thus, we propose that a similar phenomenon occurs for Fe^{3+} in the perovskite A site, in which increasing structural strain due to Fe^{3+} substitution causes a population of distorted dodecahedral sites. The M1 component also has hyperfine parameters more characteristic of Fe^{3+} in 4-coordination. If structural distortion in the A site causes some Fe^{3+}_{A} cations to interact strongly with only 4 out of the 12 nearest neighbor O^{2-} anions due to this distortion, it may explain the unusually low IS for the M1 component. The fact that the M1:M2 area ratio is extremely close to 1:2 in both of the Al-free samples may also indicate that structural distortion could break the symmetry of the A site and create an undistorted A1 site and a distorted A2 site at a consistent 1:2 stoichiometry. Such a structural distortion is not unreasonable in light of the increased unit-cell anisotropy observed by Catalli et al. (2010) for Fe^{3+}-bearing Mg-Pv.

The assignment of both the M1 and M2 doublets to Fe^{3+}_{A} is further supported by the microprobe data for these samples. In both of the Al-free samples, the (M1+M2)/M3 area ratio is in excellent agreement with the A:B occupancy ratio for Fe^{3+} inferred from the microprobe measurements (Table 2). Fe^{3+} occupancy in sample Pv05-05-57 (which also contained Al) cannot be unambiguously inferred from the microprobe data, since various degrees of mixing Al and Fe^{3+} between the A and B sites can produce identical measurements. However, the (M1+M2):M3 area ratio was relatively close to 1:1 in the Mössbauer spectra of samples Pv05-57f (4.0 mol% Fe^{3+}) and Pv05-05-57 (4.0 mol% Fe^{3+} + 5.5 mol% Al). This indicates that both Al and Fe^{3+} mix evenly between the A and B sites in the Mg-Pv structure, in agreement with the in situ synchrotron Mössbauer measurements by Catalli et al. (2011). Thus, the presence of Al does not appear to significantly alter the site occupancy of Fe^{3+} in Mg-Pv, even though the B site is expected to accommodate Al more easily than Fe^{3+}. These results are in conflict with those of Vanpeteghem et al. (2006a), who concluded that Al resides exclusively in the A site and forces Fe^{3+} into the B site. Single-crystal diffraction measurements on these samples will address this issue in greater detail in a future publication.

Power X-ray diffraction

The X-ray diffraction peaks of the quenched samples could all be indexed to either the orthorhombic perovskite structure (space group *Pbnm*), stishovite, or platinum. In some diffraction patterns the (111) line of Pt from the capsule could be observed, but this did not interfere with analysis of the perovskite. Although small amounts of MgO were observed under SEM, no MgO lines were detected in the diffraction data for any of the samples, indicating that the amount of MgO was below the detection limit (typically ~2 wt%).

Lattice parameters of the Mg-Pv for each sample are provided in Table 3. The unit-cell volumes demonstrate that incorporation of Fe^{3+} into the perovskite structure increases the volume of Mg-Pv more so than substitution of Fe^{2+}, in agreement with the results of Catalli et al. (2010). The addition of 5 mol% Al to Fe^{3+}-bearing Mg-Pv did not significantly alter the volume. Figure 6 compares the effects of Fe^{2+}, Fe^{3+}, and Fe^{3+} + 5% Al on the room-pressure volume of Mg-Pv according to this and several other studies.

The relative volumes of Fe^{3+}- and Fe^{2+}-bearing perovskites initially seem inconsistent with the fact that the high-spin crystal ionic radius for $^{VI}Fe^{3+}$ (0.785 Å) is significantly smaller than that of $^{VI}Fe^{2+}$ (0.92 Å) (Shannon 1976). However, our substitution model and Mössbauer data have shown that Fe^{3+} initially substitutes predominantly into the B site, especially at Fe^{3+} concentrations between 0.04 and 0.05, while Fe^{2+} is known to substitute

TABLE 3. Lattice parameters of six samples of $(Mg,Fe^{3+})(Si,Fe^{3+})O_3$ perovskite measured by Rietveld refinement of X-ray diffraction data

	Pv05*	Pv05-57e†	Pv10*	Pv05-05-57‡	Pv10-57†	Pv05-57f‡
a (Å)	4.7869(5)	4.782(1)	4.780(3)	4.7813(2)	4.776(3)	4.7838(2)
b (Å)	4.9381(6)	4.940(1)	4.963(4)	4.9370(3)	4.945(3)	4.9408(2)
c (Å)	6.9098(6)	6.909(1)	6.896(2)	6.9178(3)	6.912(2)	6.9154(3)
V (Å^3)	163.34(2)	163.18(5)	163.6(2)	163.30(2)	163.2(2)	163.45(2)

* Powder diffraction, Smithsonian Institution.
† Powder diffraction, APS.
‡ Single-crystal diffraction, Virginia Tech.

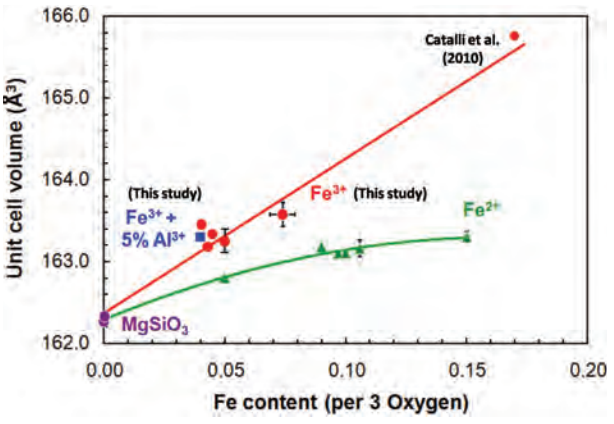

FIGURE 6. Unit-cell volumes of Mg-Pv as a function of Fe content for end-member $MgSiO_3$ (purple circles), Fe^{2+} substitution (green triangles), Fe^{3+} substitution (red circles), and Fe^{3+} substitution with 5% Al (blue squares). Points without error bars have errors smaller than the symbol. Data sources: Mg end-member: Wang et al. (1994) and Lundin et al. (2008); Fe^{2+}: Parise et al. (1990), Fei et al. (1994), Wang et al. (1994), Lundin et al. (2008); Fe^{3+}: this work and Catalli et al. (2010); Fe^{3+} + 5% Al: this work. (Color online.)

exclusively into the A site (Kudoh et al. 1990; Parise et al. 1990; Farges et al. 1994; Fei et al. 1994; Jephcoat et al. 1999). Thus, the substitution of $^{VI}Fe^{3+}$ (0.785 Å) for $^{VI}Si^{4+}$ (0.54 Å) is proportionally a much larger increase in site radius than that of $^{VIII}Fe^{2+}$ (1.06 Å) for $^{VIII}Mg^{2+}$ (1.03 Å), explaining the enhanced volume of Fe^{3+}-bearing perovskites relative to the Mg end-member or Fe^{2+}-bearing Mg-Pv. Interestingly, a linear extrapolation of our volume data out to 17 mol% Fe^{3+} is in very good agreement with the zero pressure volume at this composition measured by Catalli et al. (2010). This suggests that continued addition of Fe^{3+} to the Mg-Pv structure induces unit-cell expansion at a constant rate of roughly 0.2 $Å^3$ for each mol% Fe. In contrast, structural relaxation appears to diminish the volumetric expansion of Mg-Pv upon continued addition of Fe^{2+}.

The increased volume of the BO_6 octahedra in Fe^{3+}-bearing perovskites also explains their enhanced compressibility, both in the absence of Al (Catalli et al. 2010) and presence of Al (Catalli et al. 2011). Because individual polyhedral units display increased compressibility with increasing volume (Hazen and Finger 1979), the incorporation of significant Fe^{3+} into the B site will increase the compressibility of the octahedral framework, and of the overall structure. In addition, the compression model for perovskites developed by Angel et al. (2005) predicts that when BO_6 polyhedra are less compressible than AO_{12} polyhedra, high pressure leads to increased tilting of the octahedra, and distortion of the dodecahedra. In contrast, when BO_6 polyhedra are more compressible than AO_{12} polyhedra, volume reduction is accommodated by shrinking the octahedra, and octahedral tilting instead decreases with pressure. Although Mg-Pv obeys the former scenario (Vanpeteghem et al. 2006b), in the context of this model our volume data imply that incorporation of Fe^{3+} into Mg-Pv will make octahedra more compressible, reduce the amount of octahedral tilting with pressure, and help to stabilize the orthorhombic perovskite structure at lower mantle conditions.

CONCLUDING REMARKS

Our results demonstrate that at least 7.4 mol% of Fe^{3+} can be incorporated into the structure of magnesium silicate perovskite using standard multi-anvil synthesis. Microprobe analyses of samples with varying Fe^{3+} content suggest that at low Fe^{3+} content (4–5 mol%), Fe^{3+} substitutes into the structure using a combination of charge-coupled substitution, and B-site occupancy coupled with O vacancies. At higher Fe^{3+} content (e.g., 7.4 mol%), Fe^{3+} incorporation occurs through a combination of charge-coupled substitution, and A-site occupancy coupled with Mg vacancies. Mössbauer spectroscopy quantitatively validates this substitution mechanism, and also indicates the presence of A sites with differing degrees of anisotropic distortion. Fe^{3+} enlarges the unit-cell volume of perovskite due to this ion's significant substitution into the octahedral framework, in contrast with exclusively Fe^{2+}-bearing perovskites. The incorporation of Al into Fe^{3+}-bearing Mg-Pv does not appear to influence the behavior of Fe^{3+}.

The shift in site occupancy with increasing Fe^{3+} content may affect the spin transition of Fe^{3+} in the lower mantle. Our results imply that as Fe^{3+} content increases with depth, occupancy of Fe^{3+} will tend to shift from the B site to the A site (but only assuming that the effect of pressure does not completely eliminate the Mg occupancy substitution mechanism). Catalli et al. (2010) report that a high-spin (HS) to low-spin (LS) transition in Fe^{3+}_B is complete by 60 GPa, but no spin transition occurs for Fe^{3+}_A up to a pressure of 136 GPa. This spin behavior is similar to theoretical predictions for the Fe^{2+} ion by Cohen et al. (1997), who calculated that a spin transition would not occur in the A site until 1 TPa. Thus, to whatever extent the shift in site occupancy occurs, Fe^{3+}-bearing Mg-Pv in the deep mantle will be replenished with a population of HS-Fe^{3+}_A while being depleted of LS-Fe^{3+}_B.

The dynamics of the site occupancy and spin transition behavior may be gradual enough to avoid producing detectable boundaries. However, if the Fe^{3+} content of the lowermost mantle is high, and the preferred site occupancy of Fe^{3+} in Mg-Pv exhibits a threshold behavior, it is possible that this behavior is responsible for a portion of the seismic discontinuities recently observed below depths of ~2000 km (e.g., Thomas et al. 2004; Hutko et al. 2006; Lay et al. 2006; Van der Hilst et al. 2007). Further investigation of the effects of Fe^{3+} on the density and bulk modulus of Mg-Pv at high pressure, together with high precision in situ X-ray diffraction and Mössbauer spectroscopic measurements, is necessary to fully explain the influence of Fe^{3+} in the lower mantle.

ACKNOWLEDGMENTS

This work was supported by NSF grant EAR-0809539 (Y.F.) and the Carnegie Institution of Washington. Use of the Advanced Photon Source, an Office of Science User facility operated for the U.S. Department of Energy (DOE) Office of Science by Argonne National Laboratory, was supported by the U.S. DOE under Contract No. DE-AC02-06CH11357. We thank John Armstrong, Scott Price, and Bjorn Mysen of the Geophysical Laboratory for their assistance with instrumentation used in this study. We also thank Katherine Crispin and Stephen Gramsch for helpful reviews of this manuscript.

REFERENCES CITED

Amthauer, G., Annersten, H., and Hafner, S.S. (1976) Mössbauer spectrum of Fe-57 in silicate garnets. Zeitschrift für Kristallographie, 143, 14–55.

Andrault, D. and Bolfan-Casanova, N. (2001) High-pressure phase transformations in the $MgFe_2O_4$ and Fe_2O_3-$MgSiO_3$ systems. Physics and Chemistry of

Minerals, 28, 211–217.
Angel, R.J., Zhao, J., and Ross, N.L. (2005) General rules for predicting phase transitions in perovskites due to octahedral tilting. Physical Review Letters, 95, 025503.
Auzende, A.L., Badro, J., Ryerson, F.J., Weber, P.K., Fallon, S.J., Addad, A., Siebert, J., and Fiquet, G. (2008) Element partitioning between magnesium silicate perovskite and ferropericlase: New insights into bulk lower-mantle geochemistry. Earth and Planetary Science Letters, 269, 164–174.
Bertka, C.M. and Fei, Y. (1997) Mineralogy of the Martian interior up to core-mantle boundary pressures. Journal of Geophysical Research, 102, 5251–5264.
Catalli, K., Shim, S.H., Prakapenka, V.B., Zhao, J., Sturhahn, W., Chow, P., Xiao, Y., Liu, H., Cynn, H., and Evans, W.J. (2010) Spin state of ferric iron in $MgSiO_3$ perovskite and its effect on elastic properties. Earth and Planetary Science Letters, 289, 68–75.
Catalli, K., Shim, S.H., Dera, P., Prakapenka, V.B., Zhao, J., Sturhahn, W., Chow, P., Xiao, Y., Cynn, H., and Evans, W.J. (2011) Effects of the Fe^{3+} spin transition on the properties of aluminous perovskite—New insights for lower mantle seismic heterogeneities. Earth and Planetary Science Letters, 310, 293–302.
Cohen, R.E., Mazin, I.I., and Isaak, D.G. (1997) Magnetic collapse in transition metal oxides at high pressure: Implications for the earth. Science, 275, 654–657.
Eeckhout, S.G., Castaneda, C., Ferreira, A.C.M., Sabioni, A.C.S., de Grave, E., and Vasconcelos, D.C.L. (2002) Spectroscopic studies of spessartine from Brazilian pegmatites. American Mineralogist, 87, 1297–1306.
Farges, F., Guyot, F., Andrault, D., and Wang, Y.B. (1994) Local-structure around Fe in $Mg_{0.9}Fe_{0.1}SiO_3$ perovskite—An X-ray absorption spectroscopy study at Fe-K edge. European Journal of Mineralogy, 6, 303–312.
Fei, Y. and Bertka, C.M. (1999) Mantle Petrology: Field Observations and High Pressure Experimentation (a Tribute to Francis R. (Joe) Boyd). Edited by Y. Fei, C.M. Bertka, and B.O. Mysen, p. 189–207. Geochemical Society Special Publication 6, The Geochemical Society, Houston, Texas.
Fei, Y., Virgo, D., Mysen, B.O., Wang, Y., and Mao, H.K. (1994) Temperature-dependent electron delocalization in $(Mg,Fe)SiO_3$ perovskite. American Mineralogist, 79, 826–837.
Frost, D.J. and Langenhorst, F. (2002) The effect of Al_2O_3 on Fe-Mg partitioning between magnesiowustite and magnesium silicate perovskite. Earth and Planetary Science Letters, 199, 227–241.
Frost, D.J., Liebske, C., Langenhorst, F., McCammon, C.A., Tronnes, R.G., and Rubie, D.C. (2004) Experimental evidence for the existence of iron-rich metal in the earth's lower mantle. Nature, 428, 409–412.
Geiger, C.A., Grodzicki, M., and Amthauer, G. (2003) The crystal chemistry and Fe-II-site properties of aluminosilicate garnet solid solutions as revealed by Mössbauer spectroscopy and electronic structure calculations. Physics and Chemistry of Minerals, 30, 280–292.
Grew, E.S., Halenius, U., and Pasero, M. (2008) The crystal chemistry of aenigmatite revisited: electron microprobe data, structure refinement and Mössbauer spectroscopy of aenigmatite from Vesteroya (Norway). European Journal of Mineralogy, 20, 983–991.
Grocholski, B., Shim, S.H., Sturhahn, W., Zhao, J., Xiao, Y., and Chow, P.C. (2009) Spin and valence states of iron in $(Mg_{0.8}Fe_{0.2})SiO_3$ perovskite. Geophysical Research Letters, 36, L24303.
Hazen, R.M. and Finger, L.W. (1979) Bulk modulus-volume relationship for cation-anion polyhedra. Journal of Geophysical Research, 84, 6723–6728.
Hsu, H., Umemoto, K., Blaha, P., and Wentzkovitch, R.M. (2010) Spin states and hyperfine interactions of iron in $(Mg,Fe)SiO_3$ perovskite under pressure. Earth and Planetary Science Letters, 294, 19–26.
Hutko, A.R., Lay, T., Garnero, E.J., and Revenaugh, J. (2006) Seismic detection of folded, subducted lithosphere at the core-mantle boundary. Nature, 441, 333–336.
Jackson, J.M., Sturhahn, W., Shen, G., Zhao, J., Hu, M.H., Errandonea, D., Bass, J.D., and Fei, Y. (2005) A synchrotron Mössbauer spectroscopy study of $(Mg,Fe)SiO_3$ perosvksite up to 120 GPa. American Mineralogist, 90, 199–205.
Jephcoat, A.P., Hriljac, J.A., McCammon, C.A., O'Neill, H.St.C., Rubie, D.C., and Finger, L.W. (1999) High-resolution synchrotron X-ray powder diffraction and Rietveld structure refinement of two $(Mg_{0.95}Fe_{0.05})SiO_3$ perovskite samples synthesized under different oxygen fugacity conditions. American Mineralogist, 84, 214–220.
Knittle, E. and Jeanloz, R. (1987) Synthesis and equation of state of $(Mg,Fe)SiO_3$ perovskite over 100 GPa. Science, 235, 669–670.
Kudoh, Y., Prewitt, C.T., Finger, L.W., Darovskikh, A., and Ito, E. (1990) Effect of iron on the crystal structure of $(Mg,Fe)SiO_3$ perovskite. Geophysical Research Letters, 17, 1481–1484.
Larson, A.C. and Von Dreele, R.B. (2000) General Structure Analysis System (GSAS) (Report LAUR 86-748). Los Alamos National Laboratory, New Mexico.
Lauterbach, S., McCammon, C.A., van Aken, P., Langenhorst, F., and Seifert, F. (2000) Mössbauer and ELNES spectroscopy of $(Mg,Fe)(Si,Al)O_3$ perovskite: a highly oxidized component of the lower mantle. Contributions to Mineralogy and Petrology, 138, 17–26.
Lay, T., Hernlund, J., Garnero, E.J., and Thorne, M.S. (2006) A post-perovskite lens and D" heat flux beneath the central Pacific. Science, 314, 1272–1276.
Lundin, S., Catalli, K., Santillan, J., Shim, S.H., Prakapenka, V.B., Kunz, M., and Meng, Y. (2008) Effect of Fe on the equation of state of mantle silicate perovskite over 1 Mbar. Physics of the Earth and Planetary Interiors, 168, 97–102.
Martinez, I., Wang, Y., Guyot, F., Liebermann, R.C., and Doukhan, J.C. (1997) Microstructures and iron partitioning $(Mg,Fe)SiO_3$ perovskite–(Mg,Fe)O magnesiowustite assemblages, an analytical transmission electron microscopy study. Journal of Geophysical Research, 102, 5265–5280.
McCammon, C.A. (1997) Perovskite as a possible sink for ferric iron in the lower mantle. Nature, 387, 694–696.
McCammon, C.A., Lauterbach, S., Seifert, F., Langenhorst, F., and van Aken, P.A. (2004) Iron oxidation state in lower mantle mineral assemblages I. Empirical relations derived from high-pressure experiments. Earth and Planetary Science Letters, 222, 435–449.
Parise, J.B., Wang, Y., Yeganeh-Haeri, A., Cox, D.E., and Fei, Y. (1990) Crystal structure and thermal expansion of $(Mg,Fe)SiO_3$ perovskite. Geophysical Research Letters, 17, 2089–2092.
Pauling, L. (1929) The principles determining the structure of complex ionic crystals. Journal of the American Chemical Society, 51, 1010–1026.
Shannon, R.D. (1976) Revised effective ionic radii and systematic studies of interatomic distances in halides and chalcogenides. Acta Crystallographica A, 32, 751–767.
Sharma, P.U., Modi, K.B., and Lakhani, V. (2007) Mössbauer spectroscopic studies of Fe^{3+} substituted YIG. Ceramics International, 33, 1543–1546.
Taran, M.N., Dyar, M.D., and Matsyuk, S.S. (2007) Optical absorption study of natural garnets of almandine-skiagite composition showing intervalence $Fe^{2+} + Fe^{3+} \rightarrow Fe^{3+} + Fe^{2+}$ charge transfer transition. American Mineralogist, 92, 753–760.
Thomas, C., Garnero, E.J., and Lay, T. (2004) High-resolution imaging of lowermost mantle structure under the Cocos plate. Journal of Geophysical Research, 109, B08307.
Van der Hilst, R.D., de Hoop, M.V., Wang, P., Shim, S.H., Ma, P., and Tenorio, L. (2007) Seismostratigraphy and thermal structure of Earth's core-mantle boundary region. Science, 315, 1813–1817.
Vanpeteghem, C.B., Angel, R.J., Ross, N.L., Jacobsen, S.D., Dobson, D.P., Litasov, K.D., and Ohtani, E. (2006a) Al, Fe substitution in the $MgSiO_3$ perovskite structure: A single crystal X-ray diffraction study. Physics of the Earth and Planetary Interiors, 155, 96–103.
Vanpeteghem, C.B., Zhao, J., Angel, R.J., Ross, N.L., and Bolfan-Casanova, N. (2006b) Crystal structure and equation of state of $MgSiO_3$ perovskite. Geophysical Research Letters, 33, L03306.
Wang, Y., Weidner, D.J., Liebermann, R.C., and Zhao, Y. (1994) P-V-T equation of state of $(Mg,Fe)SiO_3$ perovskite: constraints on composition of the lower mantle. Physics of the Earth and Planetary Interiors, 83, 13–40.
Woodland, A.B. and O'Neill, H.St.C. (1993) Synthesis and stability of $Fe_3^{2+}Fe_2^{3+}Si_3O_{12}$ garnet and phase relations with $Fe_3^{2+}Al_2Si_3O_{12}$-$Fe_3^{2+}Fe_2^{3+}Si_3O_{12}$ solutions. American Mineralogist 78, 1002–1015.
Woodland, A.B., Bauer, M., Boffa Ballaran, T., and Hanrahan, M. (2009) Crystal chemistry of $Fe_3^{2+}Cr_2Si_3O_{12}$-$Fe_3^{2+}Fe_2^{3+}Si_3O_{12}$ garnet solid solutions and related spinels. American Mineralogist, 94, 359–366.
Zhang, F. and Oganov, A.R. (2006) Valence state and spin transitions of iron in Earth's mantle silicates. Earth and Planetary Science Letters, 249, 436–443.

Manuscript received February 24, 2012
Manuscript accepted August 3, 2012
Manuscript handled by M. Darby Dyar